NASA TECHNICAL MEMORANDUM

NASA TM X-73542

NASA TM X-73542

EFFECTS OF FORWARD VELOCITY ON NOISE FOR A J85 TURBOJET ENGINE WITH MULTITUBE SUPPRESSOR FROM WIND TUNNEL AND FLIGHT TESTS

by James R. Stone, Jeffrey H. Miles,
and Noel B. Sargent
Lewis Research Center
Cleveland, Ohio 44135

TECHNICAL PAPER to be presented at the
Ninety-second Meeting of the
Acoustical Society of America
San Diego, California, November 16-19, 1976

EFFECTS OF FORWARD VELOCITY ON NOISE FOR A J85 TURBOJET ENGINE WITH MULTITUBE SUPPRESSOR FROM WIND TUNNEL AND FLIGHT TESTS

by James R. Stone, Jeffrey H. Miles, and Noel B. Sargent

Lewis Research Center

E-8974

ABSTRACT

Flight and wind tunnel noise tests were conducted using a J85 turbojet engine as a part of comprehensive programs to obtain an understanding of forward velocity effects on jet exhaust noise. Nozzle configurations of primary interest were a 104-tube suppressor with and without an acoustically-treated shroud. The installed configuration of the engine was as similar as possible in the flight and wind tunnel tests. Some differences necessarily existed, however; e.g., for the flight tests the engine was in motion with respect to the microphones, and for the wind tunnel test it was not. Exact simultaneous matching of engine speed, exhaust velocity, and exhaust temperature was not possible, and the wind tunnel maximum Mach number was ~0.27, while the flight Mach number was ~0.37. The nominal jet velocity range was 450 to 640 m/sec. For both experiments, background noise limited the jet velocity range for which significant data could be obtained. In the present tests the observed directivity and forward velocity effects for the suppressor are more similar to predicted trends for internally-generated noise than unsuppressed jet noise.

INTRODUCTION

The development of an environmentally and economically acceptable advanced supersonic cruise airplane will require substantial advancements in jet engine noise suppression technology. Such advancements will be based

STAR category 71

largely on model and full-scale static tests, since flight tests are too costly. Therefore, it is essential to be able to predict the noise in flight from static or simulated-flight test data. Early noise predictions generally assumed that jet noise is simply a function of the relative jet velocity, $V_r = V_j - V_o$, i.e., OASPL $\propto 10 \log V_r^n$ indicating significant reductions in noise with increasing airplane velocity, V_o, at constant jet velocity, V_j. (All symbols are defined in the appendix.) Experimental results, however, indicate that such a simplified model overpredicts the noise reduction in flight, even for an unsuppressed jet.

In past developments of jet noise suppressors, noise measurements have been made in flight and the results compared with static ground test data (e.g., refs. 1 to 7). These tests have usually confirmed the reduction of peak jet noise with forward velocity, but the magnitude of this reduction has varied for different nozzle types. Other noise tests have attempted to determine forward velocity effects by operating the test nozzles in wind tunnels (e.g., refs. 8 and 9) or in a free jet (e.g., refs. 10 to 15). All these tests are limited to various degrees by experimental difficulties. Some of these difficulties will be considered in greater detail in describing the experiments and results of this study.

In order to obtain a better understanding of the various effects of forward velocity on jet noise suppression, flight and wind tunnel noise tests were conducted with a J85 engine using representative exhaust noise suppressors. It is also the purpose of this study to evaluate some of the capabilities and limitations of these two experimental methods, so that future experiments on forward velocity effects can be conducted in the most effective manner. The nozzle configuration of primary interest in this study is a 104-elliptical-tube suppressor, based on a design shown in reference 16, with and without an acoustically-lined shroud.

The flight tests were conducted by the NASA Lewis Research Center at the Selfridge Air National Guard Base using an F-106B airplane modified to carry two under-wing nacelles, each containing a calibrated J85-13 engine (ref. 17). The wind tunnel tests were conducted by the NASA Ames Research Center in the 12- by 24-m (40- by 80-ft) wind tunnel (refs. 18 and 19).

In addition, both Centers performed static tests to provide a baseline for acoustic comparisons. The nominal jet velocity range for all these tests was 450 to 640 m/sec (~1.6-2.1 times the ambient sonic velocity, c_a). The installed configuration of the engine including the inlet was as similar as possible in the two test programs. Some differences necessarily existed, however; e.g., the flight Mach number was about 0.37, while the wind tunnel free-stream Mach number ranged from near 0 to about 0.27. Furthermore, for the flight tests the engine was in motion with respect to the microphone, and for the wind tunnel tests it was not. An additional complication was that for the wind tunnel tests a J85-5 engine was used because of damage to the J85-13. The main difference between the two engines is that the J85-13 had an afterburner section (although the afterburner itself was removed), so a dummy section was used with the J85-5 to give the same nacelle length. Because of the differences in engine performance, exact simultaneous matching of engine speed, exhaust velocity and exhaust temperature was not possible. For both experiments, background noise limited the jet velocity range for which significant data could be obtained. Additional problem areas for the wind tunnel were reverberations due to tunnel wall reflections and acoustic near-field limitations. The flight tests were complicated by ground reflections, difficulty in accurately determining airplane position, and the inherently transient nature of the data.

EXPERIMENTAL APPARATUS AND PROCEDURE

The angular conventions and geometric nomenclature used herein are illustrated in figure 1.

Engine and Nozzle Configurations

Engine. - The present tests were all conducted with J85 turbojet engines. The same calibrated J85-13 engine was used for the airplane static

and flight tests and for the wind tunnel tests conducted without an airplane model (isolated nacelle). However, this engine was damaged during the wind tunnel tests. Consequently, the wind tunnel tests with the airplane model and all of the outdoor engine stand tests were conducted with a J85-5 engine. The results which will be discussed herein are for the airplane static and flight tests and for the airplane-model test in the wind tunnel and on the outdoor test stand.

Nozzle. - A photograph of the 104-elliptical-tube nozzle (without shroud) mounted on the airplane is shown in figure 2(a). (A more detailed description of the nozzle and also the lined ejector shroud can be found in ref. 17.) The shroud support structure was in place as shown for the tests. The elliptical tubes have a common exit plane and are mounted on a conical baseplate with their major axes oriented radially. The ratio of the circular area just circumscribing the outer tubes to the total jet exit area is 2.8. (In a possible application of this concept, the array of tubes might consist of four or more segments, which would be removed from the exhaust stream and stowed in the shroud during cruise; however, the test nozzle was of fixed geometry.)

Figure 2(b) shows a photograph of the acoustically-treated shroud installed on the 104-tube nozzle mounted on the airplane. The shroud had an exit diameter of 53.8 cm and extended 73.6-cm beyond the tube exit plane. The acoustic treatment consisted of a perforated sheet with 23 percent open area adjacent to the exhaust gases, a bulk absorber, and a solid backing sheet.

The reference nozzle of references 17 to 19 is not included in this study because it was found to exhibit noise levels higher than those of a convergent conical nozzle.

Wind Tunnel Tests

The NASA Ames 12- by 24-m wind tunnel as an acoustics facility is described in more detail in references 18 and 19, so only a brief description of the test set-up and data reduction is given herein.

Apparatus. - The airplane-model installation of the 104-tube suppressor nozzle with its acoustically treated shroud is shown installed in the wind tunnel in figure 3. (The airplane-model installation is termed wing-nacelle in refs. 18 and 19.) The microphones were positioned 4.20 m from the engine centerline (at zero angle of attack) in the $\varphi = 0^{o}$ (flyover) plane. The engine centerline was 6.1 m above the tunnel floor. The engine is shown mounted on the tunnel test/thrust stand (fig. 3). The two front struts provided the main support; the rear strut was used for stabilization and to change the angle of attack. For static testing in the tunnel, a bellmouth inlet was used. With the wind tunnel on, a sharp-lip, flight-type inlet was used. A schematic of the microphone array is shown in figure 4. Note that microphones numbers 1 through 7 and 14 were staggered ±10 cm on each side of the engine centerline in order to keep a given microphone out of the wake of the microphone immediately upstream. There are slight differences in microphone position relative to the noise source due to the slightly different exit plane locations with and without the shroud. These microphones (and those at the wind-tunnel positions during the outdoor tests) were equipped with nose cones and were pointed directly into the free-stream flow.

Data reduction. - The processing of the acoustic data in reference 18 consisted of applying corrections for system response characteristics, background noise, and reverberations. The background noise (engine off) at each position for each free-stream velocity was antilogarithmically subtracted from the measured SPL's. The reverberation corrections were obtained for each position by comparing wind-tunnel static data with outdoor static data (corrected for ground reflections according to ref. 20). Neither reference 18 or 19 made any corrections based on the near-field position of the wind tunnel microphones or for the downstream convection of sound by the free stream flow. The background noise, reverberation, free-stream convection and near-field problems specifically related to this study will be further discussed in later sections.

Sound convection corrections. - With flow in the wind tunnel, the sound is convected downstream as it propagates away from the source. Thus, as illustrated in figure 5, sound emitted at an angle θ is received by the microphone at a line-of-sight angle θ_m. Furthermore, the spherical spreading loss

should be related to the distance R rather than the apparent distance R_m. The problem is analogous to the flyover case where the sound is emitted when the airplane is at θ but received when the airplane is at θ_m. The required corrections are given in reference 15. For the nomenclature of this report, the relations are as follows:

$$\theta = \cos^{-1} \frac{\cos \theta_m + M_a (1 - M_a^2 \sin^2 \theta_m)^{1/2}}{M_a \cos \theta_m + (1 - M_a^2 \sin^2 \theta_m)^{1/2}} \tag{1}$$

and

$$R = R_m (1 + M_a^2 - 2M_a \cos \theta)^{-1/2} \tag{2}$$

Flight Tests

The NASA Lewis F-106B research airplane and the flight test facilities at Selfridge Air National Guard Base are described in more detail in reference 17, so only the most important features will be covered herein. The instrumentation used to obtain additional data not reported in reference 17 will be described in somewhat more detail.

Apparatus. - Two different ground stations were used for these tests. Figure 6 shows the microphone and airplane spotter positions at each ground station. The airplane was flown over the test sites at an altitude of about 90 m. Tests of the 104-tube nozzle with shroud were conducted at the north site (fig. 6(a)), while the tests without the shroud were conducted at the south site (fig. 6(b)). The data of reference 17 were obtained with a single 2.54-cm ceramic microphone 1.22-m above the concrete surface, directly under the flight path. For the supplementary data obtained in this study (not included in ref. 17) an additional array of three 1.27-cm condenser microphones was used at each ground station to provide a check of the data of reference 17. These data were used herein only to check the data of reference 17. (However, these data were made available to the General Electric Company for

use in a DOT-sponsored study and are reported in ref. 21.) Directly under the nominal flight path at least one of these microphones was 0.97-m off the concrete surface, and one was only about 5 cm off the ground, a little more than the thickness of the windscreen. All microphones were oriented for grazing incidence from the nominal flight path except the sideline microphone at the south site (fig. 6(b)), which was oriented parallel to the ground and normal to the nominal flight path.

The 2.54-cm ceramic microphone with windscreen (used for the data of ref. 17) had a flat response within ±2 dB for grazing incidence over the frequency range used, 50 to 10 000 Hz. The microphone output and an airplane position pulse were recorded directly on magnetic tape. The 1.27-cm condenser microphones used to obtain the supplementary data of this study were fitted with windscreens and had a flat response within ±1.0 dB for normal incidence over the frequency range used, 50 to 20 000 Hz. This necessitated an incidence angle correction for the flight data. For this supplementary data, the microphone outputs and airplane position pulse were FM-recorded on tape. Each microphone and instrumentation channel were calibrated in the field before and after each test with a pistonphone.

Procedure. - The data recording process utilized an observer located directly under the flight path, 68 m ahead of the primary (ref. 17) microphone station, where a camera was also located. When the observer judged the airplane to be directly overhead, he pushed a button, which supplied a pulse to the airplane position channel and triggered a time delayed signal. The time-delayed signal triggered another pulse on the data tape when the airplane was nearly over the microphone and also caused a photograph to be taken at the same time, to give a reasonably accurate airplane position. The airplane's J75 main engine was at flight idle power during the noise measurements, and the non-research J85 engine was shut off and allowed to windmill. The J85 engine with the research nozzle was operated over a range of settings up to full military power. To allow the experimental data to be corrected for background noise, data were also obtained with both J85 engines shut off, and the J75 main engine at flight idle.

Data reduction. - The magnetic-tape data of reference 17 were played back through 1/3-octave-band filters, using a 0.1-sec averaging time. The

resulting spectral data were then recorded on incremental tape for further analysis. Unless noted otherwise, the data presented herein are corrected for background noise and ground reflections and adjusted to the nominal flight path and to standard day conditions of 288 K, 101.3 kN/m^2 abs and 70 percent relative humidity. The ground reflection correction is based on the approximate method of reference 17, which does not fully account for the discrete cancellations and reinforcements but does show proper limiting behavior at low and high frequencies. (Due to the motion of the airplane during the finite data sample time, these effects would be less than in the static case; so the errors involved in the approximate correction are considered acceptable. This procedure was also used for the airplane static data in ref. 17, but these data are not used herein.)

RESULTS AND DISCUSSION

The wind tunnel results and then the flight results will first be presented and discussed separately, and finally the results will be compared and the overall implications considered.

Wind Tunnel Results

The experimental data at or near 90° to the jet axis are examined first in order to isolate source-alteration effects, since the dynamic effects are minimized at $\theta = 90^\circ$. Thereafter, data at other angles are examined, yielding information on dynamic effects.

The effects of free-stream velocity on noise are complicated by the fact that for a given microphone at a fixed measurement angle θ_m, the emission angle θ is a function of V_a. For the comparisons shown herein θ_m is generally held constant and the results for various V_a are compared with static data interpolated to the correct emission angle, θ.

104-tube nozzle without shroud. - In order to determine to what extent the spectra for this nozzle are distorted by near-field effects, wind-tunnel data at zero free-stream velocity are compared with outdoor test stand static data, corrected for distance and interpolated to the same measurement angle, in figure 7. The angles shown are $\theta = 94^{\circ}$ (fig. 7(a)); the angle of maximum sideline noise, $\theta = 114^{\circ}$ (fig. 7(b)); and $\theta = 148^{\circ}$ (fig. 7(c)). The far-field data are corrected for atmospheric absorption, and are plotted with and without a point-source, perfect ground reflection correction. The peak SPL's, which occur at high frequencies, appear to agree reasonably well, but the peak is not well defined, since data were not obtained at frequencies above 10 kHz. Also, because of this lack of high-frequency data, meaningful OASPL's cannot be obtained, except perhaps near the jet axis (fig. 7(c)). At middle and low frequencies, the wind-tunnel data do not agree well with the far-field data, perhaps because of reverberation, near-field effects, and inaccuracies in the ground reflection corrections.

The effect of free-stream velocity on the SPL spectrum at $\theta_m = 94^{\circ}$ is shown in figure 8 for high jet velocity, $V_j/c_a > 1.7$. For each free-stream velocity, comparison spectra at zero free-stream velocity are shown for both the same V_j/c_a and the same V_r/c_a (obtained by logarithmic interpolation of the wind-tunnel static data). Even at the lowest free-stream Mach number of 0.15 (fig. 8(a)) the noise data are lost below a frequency of 400 Hz because of background noise. At the intermediate free-stream Mach number of 0.22 (fig. 8(b)), data are available only for frequencies of 2 kHz and higher. At the highest free-stream Mach number of 0.27 (fig. 8(c)), the data at $\theta_m = 94^{\circ}$ did not appear to be properly corrected (in ref. 18) for background noise, so the data for $\theta_m = 105^{\circ}$ ($\theta = 90^{\circ}$) are shown instead; only at frequencies of 2.5 kHz and higher are the SPL data considered to be valid. Within the limited range of valid data an apparent trend can be observed: the data appear to agree better when compared on the basis of a characteristic velocity intermediate between V_r and V_j rather than either V_r or V_j. However, even at the highest free-stream velocity (fig. 8(c)), the apparent SPL suppression is only about 1 dB near the peak, which is probably not significant in view of the problems involved in interpreting these data.

At angles away from $\theta = 90^{o}$, additional effects of free-stream Mach number might be expected, due to changes in source convection velocity. The effect of free-stream Mach number on the SPL spectrum at high jet velocity, $V_j/c_a > 1.7$, is shown in figure 9 for $\theta_m = 114^{o}$ (the angle of peak sideline noise) and in figure 10 for $\theta_m = 148^{o}$. For each free-stream velocity, comparison spectra at zero free-stream velocity are shown for both the same V_j/c_a and the same V_r/c_a. It is difficult to establish any consistent trend from these data, since a large part of each spectrum appears to agree with the static data at the same relative jet velocity, while the peak level, which has a strong influence on the OASPL, appears to agree better with the static data at the same absolute jet velocity.

The peak-SPL directivity patterns for various V_a/c_a, normalized to the static value at $\theta = 90^{o}$, are shown in figure 11. In the static case (fig. 11(a)), the predicted directivity for unsuppressed jet mixing noise (ref. 22) is shown for comparison. It can be seen that the directivity for the 104-tube nozzle is quite different from that of unsuppressed jet noise. Because the jet noise is substantially reduced, the possibility should be considered that internally generated noise becomes controlling (as in refs. 23 and 24). Therefore, the predicted directivity for internally-generated noise (from ref. 24) is also shown for comparison. Considering the data quality, both the static and "in-flight" directivities are similar to those expected for internally-generated noise.

104-tube nozzle with shroud. - In order to determine to what extent the spectra for this nozzle are distorted by near-field effects, wind-tunnel data at zero free-stream velocity are again compared with outdoor static data, corrected for distance (including atmospheric absorption effects) and interpolated to the same angle, in figure 12. The angles shown are $\theta = 90^{o}$ (fig. 12(a)); the angle of maximum sideline noise, $\theta = 111^{o}$ (fig. 12(b)); and $\theta = 147^{o}$ (fig. 12(c)). The far-field data are plotted with and without a point-source, perfect ground reflection correction. No consistent range of agreement can be identified, and, as with the unshrouded configuration, the spectral shape is poorly defined and meaningful OASPL's cannot be obtained, due to the lack of data for frequencies above 10 kHz, except perhaps near the jet axis (fig. 12(c)).

The effects of free-stream velocity on the SPL spectra are shown at $\theta_m = 90^o$ (fig. 13), $\theta_m = 111^o$ (the angle of maximum sideline noise, fig. 14), and $\theta_m = 147^o$ (fig. 15). For each free-stream velocity and angle, comparison spectra at zero free-stream velocity are shown for both the same V_j/c_a and the same V_r/c_a (obtained by linear logarithmic interpolation of the wind-tunnel static data). Due to the background noise problem, significant data can be obtained only at a free-stream Mach number of 0.15, except near the jet axis (fig. 15). At $\theta_m = 90^o$, the results at a free-stream Mach number of 0.15 (fig. 13(a)) are quite similar to those of the unshrouded configuration, but even less well defined. The data trends at $\theta_m = 111^o$ (fig. 14) appear inconsistent, but the $\theta_m = 147^o$ data again seem consistent with the unshrouded reshrouded results.

The peak-SPL directivity patterns for various V_a/c_a, relative to $\theta = 90^o$, are shown in figure 16. The predicted directivity for internal noise (ref. 24) is again shown for comparison, and the predicted unsuppressed jet noise directivity (ref. 22) is also shown in the static case (fig. 16(a)). As with the unshrouded configuration, the directivity is quite different from that predicted for unsuppressed jet noise. And, as was the case without the shroud, both static and "in-flight" directivities are roughly similar to those expected for internally-generated noise.

Flight Results

104-tube nozzle without shroud. - The effect of flight on the SPL spectrum at $\theta \approx 90^o$ is shown in figure 17 for a flight Mach number, $V_o/c_a \approx 0.37$, and three different jet velocities. For each jet velocity, comparison spectra are shown for both the same V_j/c_a and the same V_r/c_a (obtained by linear logarithmic interpolation or extrapolation of the outdoor engine static data of reference 18; these data are judged more reliable than the airplane static data of reference 17 because of the longer integration time used in ref. 18). The range of background noise in flight is also shown, and the experimental data are corrected for the lower limit of background noise.

As can be seen, the useable frequency range is diminished because of background noise interference. The data are significantly above the background noise only at and above frequencies of 630 Hz or higher, depending on the jet velocity. As was the case in the wind tunnel tests, it is difficult to establish any consistent trends of source alteration. Most of the spectrum appears to agree with the projected static data at the same relative jet velocity, while the peak levels, which have a strong influence on the OASPL, appear to agree better with the projected static data at the same absolute jet velocity. There is also a slight trend for a shift to lower frequency with flight; this would be consistent with scaling on the basis of a Strouhal number based on relative jet velocity, $f_c D_e/V_r$, but this trend is probably not significant within the accuracy of these data.

The static and inflight OASPL directivity patterns, normalized to the value at $\theta = 90^o$, are shown in figure 18. The directivity expected for internally-generated noise (ref. 24), both statically and in flight, is shown for comparison. Both the static and inflight directivities show some similarity to those expected for internally generated noise (ref. 24), but not as much as shown for the wind tunnel data (fig. 13). Even so, the qualitative trend of noise reduction for $\theta > 90^o$ and noise increase for $\theta < 90^o$ is as expected for noise sources moving with the airplane, rather than convecting away from it (such as turbulent eddies).

104-tube nozzle with shroud. - The effect of flight on the SPL spectrum at $\theta \approx 90^o$ for the nozzle with shroud is shown in figure 19 for a flight Mach number, $V_o/c_a \approx 0.37$, and two different jet velocities. For each jet velocity, comparison spectra are shown for both the same V_j/c_a and the same V_r/c_a (obtained by linear logarithmic interpolation or extrapolation of the outdoor engine static data of ref. 18). The range of background noise in flight is also shown. As can be seen, the useable frequency range again is decreased because of background noise interference. The data are significantly above the background noise only at frequencies of 800 Hz or higher at the high jet velocity (fig. 19(a)). Very little meaningful data can be obtained at $V_j/c_a = 1.8$ (fig. 19(b)) or lower. It appears that for the range of data shown, the flight spectra agree reasonably well in peak level with the static data at the same V_j/c_a at the higher jet velocity (fig. 19(a)).

The static and in-flight OASPL directivity patterns, normalized to the value at $\theta = 90^{o}$, are shown in figure 20. The static data show rear angle noise levels (relative to 90^{o}) greater than expected for internal noise, but still quite different from those expected for unsuppressed jet noise. However, the in-flight data show good agreement with the predicted internal noise curve (ref. 24).

Discussion

Because of the near-field and background-noise problems in the wind tunnel, the flight tests, although having accuracy problems, give a better absolute measure of the noise levels, compared with the outdoor engine stand data, than those obtained in the wind tunnel. Recent studies (e.g., ref. 25) indicate that promising methods exist for improving flight data quality. In particular, improved methods have been developed for ground reflection corrections (e.g., refs. 26-27), and experimental methods have been devised for reducing the impact of ground reflections (ref. 25).

The wind-tunnel results presented herein indicate the wind tunnel without wall treatment is quite limited as an acoustic facility for configurations like those of the current study. Because of the combination of background noise and reverberation effects, far field noise data could not be obtained in the present study. However, a recent study (ref. 28) indicates that meaningful data can be obtained from the wind-tunnel near field in conjunction with empirical near-field-to-far-field relations. In the current study the spectral shapes were distorted, so that even on a relative basis the OASPL's are not considered meaningful. With increasing free-stream Mach number, low-frequency spectral information is lost because of background noise; for the suppressor, except at angles near the jet axis, data could be obtained only for the highest frequencies at high free-stream Mach numbers.

Both wind tunnel and flight tests indicated that the 104-tube nozzle is an effective suppressor, especially when used with an acoustically-treated shroud (refs. 17 and 18). However, the flight tests showed that the noise

levels for the nozzle and the shroud were not reduced by increasing forward velocity as much as is typically expected for unsuppressed jets. Such results have often been interpreted as a loss of suppression in flight.

This so-called "loss of suppression" can be accounted for by considering the various aspects of flight effects. The effects of source motion relative to the propagation medium (dynamic effect) and relative to the observer (kinematic effect) can be conceptually separated from the effect of free-stream velocity on noise source strength. At 90° to the jet axis the relative motion effects should be minimal, thus isolating the source alteration effects. Both experimental methods indicate that the suppressor noise source strength is only slightly affected, if at all, by flight. This is shown for the wind tunnel tests in figures 8 and 13 (without and with shroud, respectively) and for the flight tests in figures 17 and 19 (without and with shroud, respectively). Therefore, the source strength reduction typically observed in flight for an unsuppressed jet is not obtained for the suppressors, leading to the "loss of suppression".

Both experimental methods indicate a noise increase in flight for $\theta < 90^{\circ}$ coupled with a noise decrease for $\theta > 90^{\circ}$. This is shown for the wind tunnel tests in figures 11 and 16 (without and with shroud, respectively) and for the flight tests in figures 18 and 20 (without and with shroud, respectively). This trend is consistent with that predicted for internally-generated noise (refs. 23 and 24). Although it cannot be stated with certainty that the internal noise is dominant, it can be stated that the directivity and flight effects of the suppressed engine are more similar to trends predicted for internal noise than for unsuppressed jet noise.

CONCLUDING REMARKS

It was found that the suppressor noise levels were not reduced as much by forward velocity as is expected for unsuppressed jets, leading to what has been termed as a "loss of suppression" in flight. The directivity and forward velocity effects for the suppressor appear to be more similar to predicted trends for internally-generated noise than for unsuppressed jet noise.

APPENDIX - SYMBOLS

c_a	ambient sonic velocity, m/sec
f	frequency in frame of reference of observer, Hz
f_c	1/3-octave-band center frequency, Hz
f_s	frequency in frame of reference of source, Hz
n	exponent for effect of V_r on OASPL, dimensionless
OASPL	overall sound pressure level, dB re 20 $\mu N/m^2$
R	distance from source to observer, m
SPL	1/3-octave-band sound pressure level, dB re 20 $\mu N/m^2$
V_a	free-stream velocity relative to nozzle, m/sec
V_j	isentropic fully-expanded jet velocity, m/sec
V_r	relative jet velocity, $V_j - V_a$, m/sec
V_o	airplane velocity relative to observer, m/sec
φ	azimuthal angle (fig. 1), degrees
θ	polar angle of noise emission relative to engine inlet axis (fig. 1), degrees
θ_m	measurement angle relative to engine inlet axis (fig. 5), degrees

Subscripts:

Bg	background noise
M	maximum

REFERENCES

1. Coles, W. D., Mihaloew, J. A., and Swan, W. H., "Ground and In-Flight Acoustic and Performance Characteristics of Jet Aircraft Exhaust Noise Suppressors," NASA TN D-874 (1961).
2. Brausch, J. F., "Flight Velocity Influence on Jet Noise of Conical Ejector, Annular Plug and Segmented Suppressor Nozzles," General Electric Co. (1972); also NASA CR-120961.
3. Burley, R. R., Karabinus, R. J., and Freedman, R. J., "Flight Investigation of Acoustic and Thrust Characteristics of Several Exhaust Nozzles Installed on Underwind Nacelles on an F106 Airplane," NASA TM X-2854 (1973).
4. Burley, R. R. and Johns, A. L., "Flight Velocity Effects on Jet Noise of Several Variations of a Twelve-Chute Suppressor Installed on a Plug Nozzle," NASA TM X-2918 (1974).
5. Burley, R. R. and Head, V. L., "Flight Velocity Effects on Jet Noise of Several Variations of a 48-Tube Suppressor Installed on a Plug Nozzle," NASA TM X-2919 (1974).
6. Bushell, K. W., "Measurement and Prediction of Jet Noise in Flight," Paper No. 75-461 (AIAA, New York, 1975).
7. Brooks, J. R. and Woodrow, R. J., "The Effects of Forward Speed on a Number of Turbojet Exhaust Silencers," Paper No. 75-506 (AIAA, New York, 1975).
8. Atencio, A., Jr. and Soderman, P. T., "Comparison of Aircraft Noise Flight Test and in the NASA Ames 40- by 80-Foot Wind Tunnel," Paper No. 73-1047 (AIAA, New York, 1973).
9. Cocking, B. J. and Bryce, W. D., "Subsonic Jet Noise in Flight Based on Some Recent Wind-Tunnel Results," Paper No. 75-462 (AIAA, New York, 1975).
10. von Glahn, U. H., Groesbeck, D. E., and Goodykoontz, J. H., "Velocity Decay and Acoustic Characteristics of Various Nozzle Geometries with Forward Velocity," Paper No. 73-629 (AIAA, New York, 1973).

11. von Glahn, U. and Goodykoontz, J., "Forward Velocity Effects on Jet Noise with Dominant Internal Noise Source," NASA TM X-71438 (1973).
12. von Glahn, U., Goodykoontz, J., and Wagner, J., "Nozzle Geometry and Forward Velocity Effects on Noise for CTOL Engine-Over-the-Wing Concept," NASA TM X-71453 (1973).
13. Packman, A. B., Ng, K. W., and Paterson, R. W., "Effects of Simulated Forward Flight on Subsonic Jet Exhaust Noise," Paper No. 75-869 (AIAA, New York, 1975).
14. de Belleval, J. F., Chen, C. Y., and Perulli, M., "Investigation of In-Flight Jet Noise Based on Measurements in an Anechoic Wind Tunnel," presented at 6th International Congress on Instrumentation and Installations for Aerospace Simulation, Ottawa, Canada, 22-24 Sept, 1975.
15. Plumblee, H. E., ed., "Effects of Forward Velocity on Turbulent Jet Mixing Noise," NASA CR-2702 (1976).
16. Swan, W. C. and Simcox, C. D., "A Status Report on Jet Noise Suppression as Seen by an Aircraft Manufacturer," Paper No. 73-816 (AIAA, New York, 1973).
17. Burley, R. R., "Flight Velocity Effects on Jet Noise of Several Variations of a 104-Tube Suppressor Nozzle," NASA TM X-3049 (1974).
18. Beulke, M. R., et al., "A Forward Speed Effects Study on Jet Noise from Several Suppressor Nozzles in the NASA/Ames 40- by 80-Foot Wind Tunnel," General Electric Co. (1974); also NASA CR-114741.
19. Atencio, A., Jr., "Wind Tunnel Measurements of Forward Speed Effects on Jet Noise from Suppressor Nozzles and Comparison with Flight Test Data," Paper No. 75-870 (AIAA, New York, 1975).
20. Hoch, R. and Thomas, P.: The Effect of Reflections on Jet Sound Pressure Spectra. First Symposium on Aeronautical Acoustics, Mar. 6-8, 1968.
21. Clapper, W. S., Mani, R., and Banerian, G., "Development of a Technique for Inflight Jet Noise Simulation - Parts I and II," Paper No. 76-532 (AIAA, New York, 1976).
22. Stone, J. R., "Interim Prediction Method for Jet Noise," NASA TM X-71618 (1974).

23. Stone, J. R., "On the Effects of Flight on Jet Engine Exhaust Noise," NASA TM X-71819 (1975).

24. Stone, James R.: Flight Effects on Exhaust Noise for Turbojet and Turbofan Engines - Comparison of Experimental Data with Prediction. NASA TM X-73552, presented at the Ninety-second Meeting of the Acoustical Society of America, San Diego, Cal., Nov. 16-19, 1976.

25. Chun, K. S., Berman, C. H., and Cowan, S. J., "Effects of Motion on Jet Exhaust Noise from Aircraft," NASA CR-2701 (1976).

26. Miles, J. H., "Analysis of Ground Reflection of Jet Noise with Various Microphone Arrays over an Asphalt Surface," NASA TM X-71696 (1975).

27. Miles, J. H., Stevens, G. H., and Leininger, G. G., "Analysis and Correction of Ground Reflection Effects in Measured Narrowband Sound Spectra Using Cepstral Techniques," NASA TM X-71810 (1975).

28. Strout, F. G., "Flight Effects on Noise Generated by the JT8D-17 Engine in a Quiet Nacelle and in a Conventional Nacelle as Measured in the NASA-Ames 40- by 80-Foot Wind Tunnel," Boeing Commercial Airplane Co. Rept. D6-42813 (1976); also NASA CR-137797.

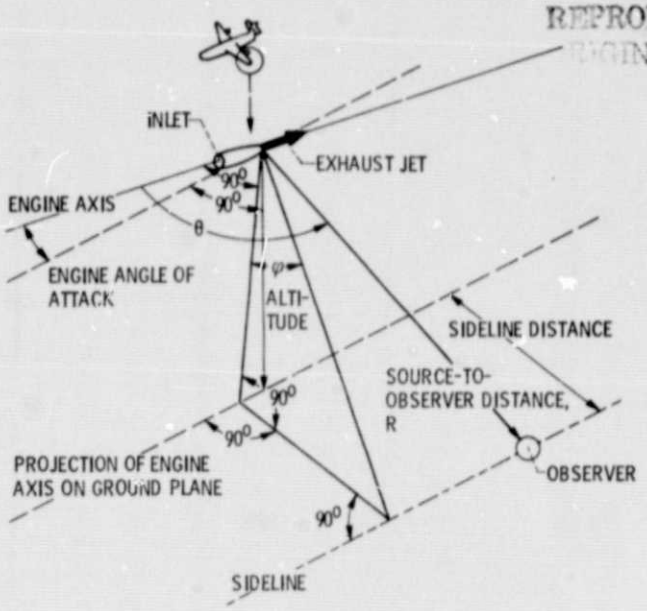

Figure 1. - Geometric variables describing position at airplane exhaust noise source with respect to an observer.

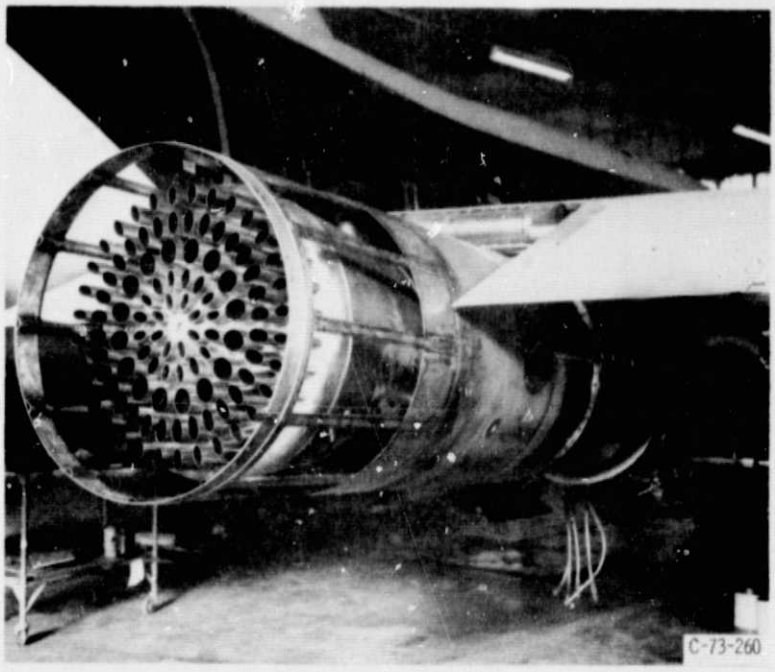

(a) WITHOUT SHROUD.

Figure 2. - 104-Elliptical-tube nozzle mounted on airplane (ref. 17).

(b) WITH ACOUSTICALLY-TREATED SHROUD.

Figure 2. - Concluded.

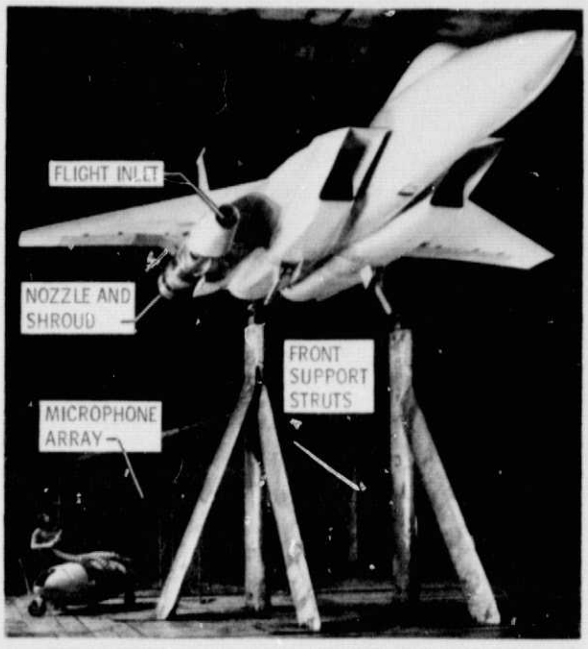

Figure 3. - Airplane-model installation of 104-eliptical-tube nozzle with acoustically-treated shroud in NASA-Ames 12- by 24-m (40-by 80-ft) wind tunnel (ref. 18).

MIC NO.	104-TUBE NOZZLE WITHOUT SHROUD: ANGLE (DEGREES) REF. 0° AT ENGINE INLET	104-TUBE NOZZLE WITHOUT SHROUD: ACOUSTIC PATH LENGTH (FT, METERS)	104-TUBE NOZZLE WITH SHROUD: ANGLE (DEGREES) REF. 0° AT ENGINE INLET	104-TUBE NOZZLE WITH SHROUD: ACOUSTIC PATH LENGTH (FT, METERS)
1	161.8	44.6 13.6	161.4	43.6 13.3
2	147.3	25.7 7.8	146.1	24.9 7.6
3	137.0	20.4 6.2	135.0	19.7 6.0
4	129.2	17.9 5.5	126.6	17.3 5.3
5	113.9	15.2 4.6	110.4	14.8 4.5
6	104.5	14.4 4.3	100.5	14.2 4.3
7	94.1	14.0 4.3	90.0	13.9 4.2
8	73.3	14.5 4.4	69.6	14.8 4.5
9	121.8	20.9 6.4	119.4	20.4 6.2
10	128.8	22.7 6.9	126.8	22.1 6.7
11	141.4	28.4 8.7	140.2	27.7 8.4
12	150.2	35.7 10.9	149.4	34.9 10.6

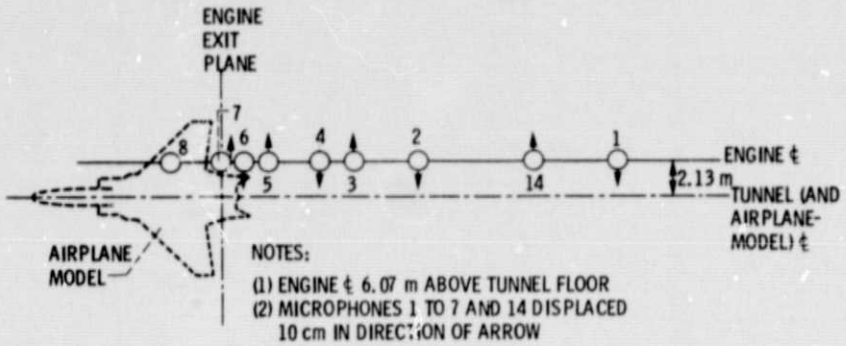

Figure 4. - Schematic diagram of microphone array for wind tunnel tests (ref. 18).

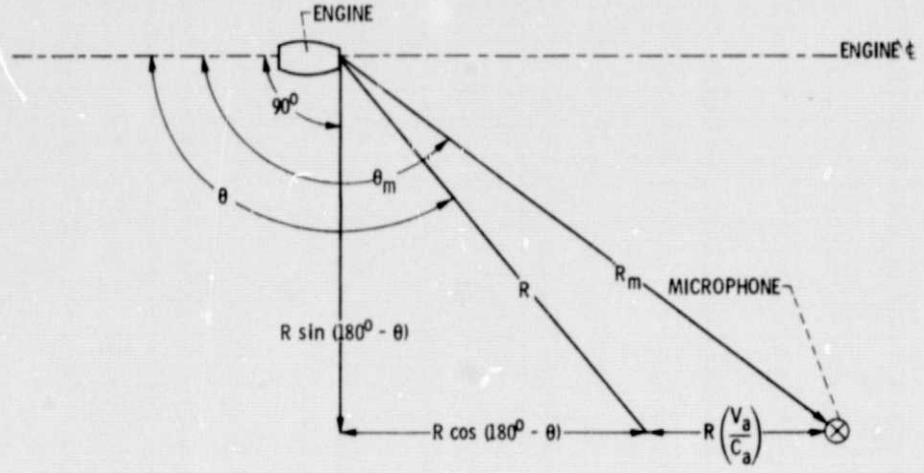

Figure 5. - Sound propagation through a moving medium: relation of emission and measurement (reception) coordinates.

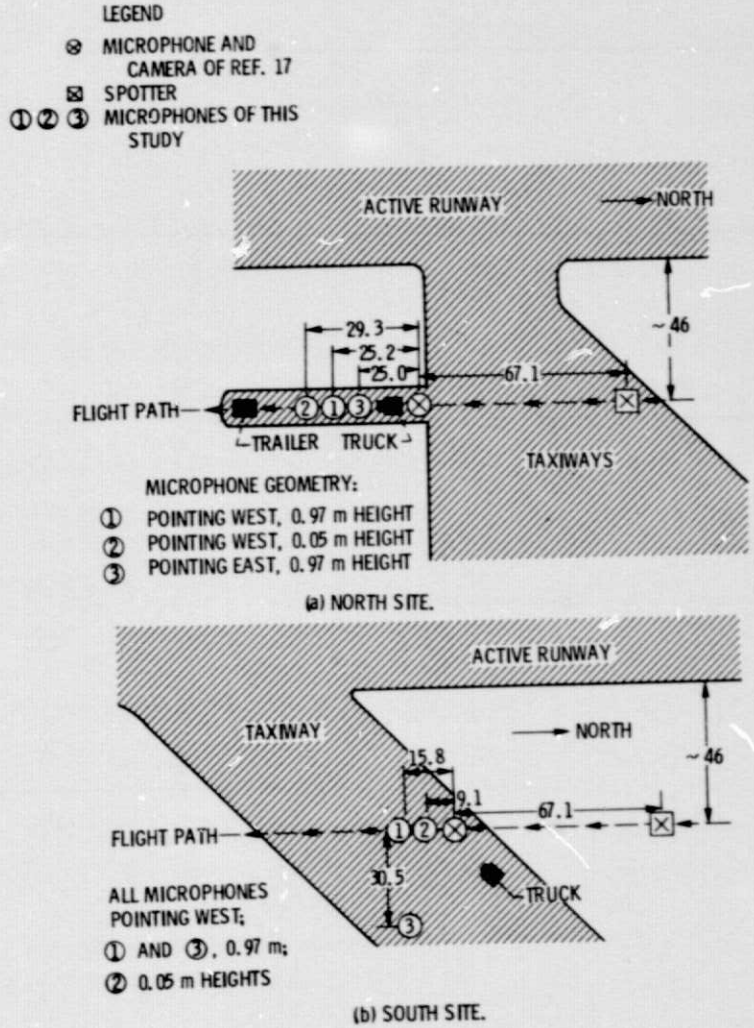

Figure 6. - Ground stations for flight tests. (Truck contains instrument power supply.)

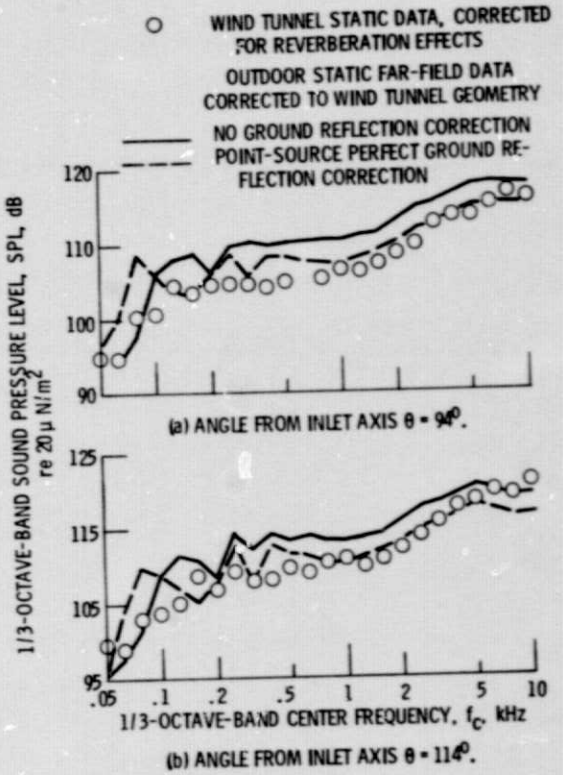

Figure 7. - Wind-tunnel nearfield effects for 104-tube nozzle without shroud. Comparison of zero free-stream velocity data with outdoor farfield results; high jet velocity, $V_j/c_a = 1.82$.

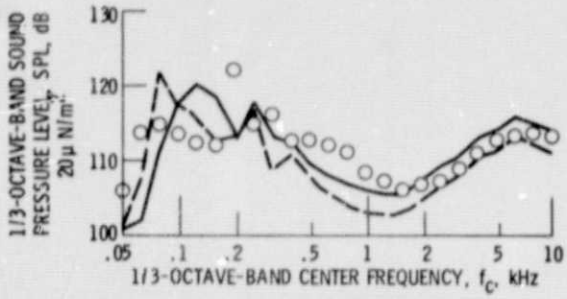

(c) ANGLE FROM INLET AXIS $\theta = 148^0$.

Figure 7. - Concluded.

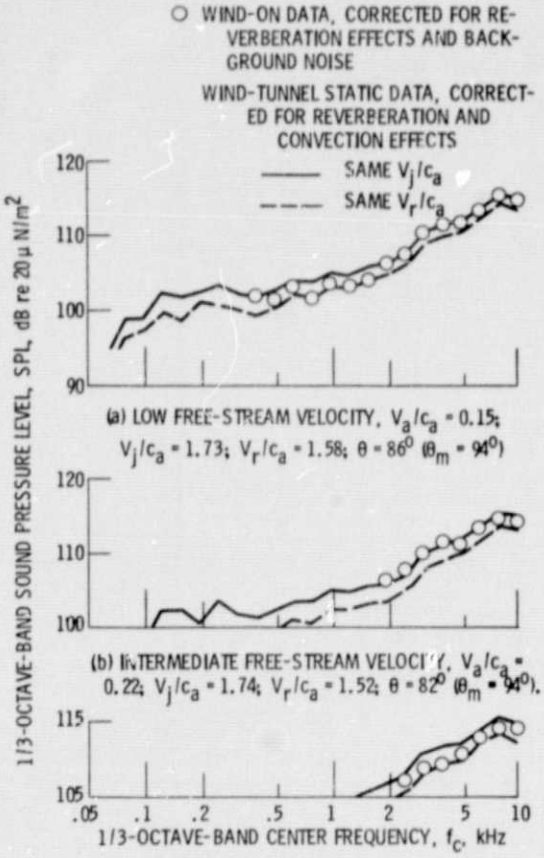

(a) LOW FREE-STREAM VELOCITY, $V_a/c_a = 0.15$; $V_j/c_a = 1.73$; $V_r/c_a = 1.58$; $\theta = 86^0$ ($\theta_m = 94^0$)

(b) INTERMEDIATE FREE-STREAM VELOCITY, $V_a/c_a = 0.22$; $V_j/c_a = 1.74$; $V_r/c_a = 1.52$; $\theta = 82^0$ ($\theta_m = 94^0$).

(c) HIGH FREE-STREAM VELOCITY, $V_a/c_a = 0.27$; $V_j/c_a = 1.71$; $V_r/c_a = 1.44$; $\theta = 90^0$ ($\theta_m = 105^0$).

Figure 8. - Effect of free-stream velocity on SPL spectra for 104-tube nozzle without shroud; high jet velocity; emission angle from inlet axis, $\theta \approx 90^0$).

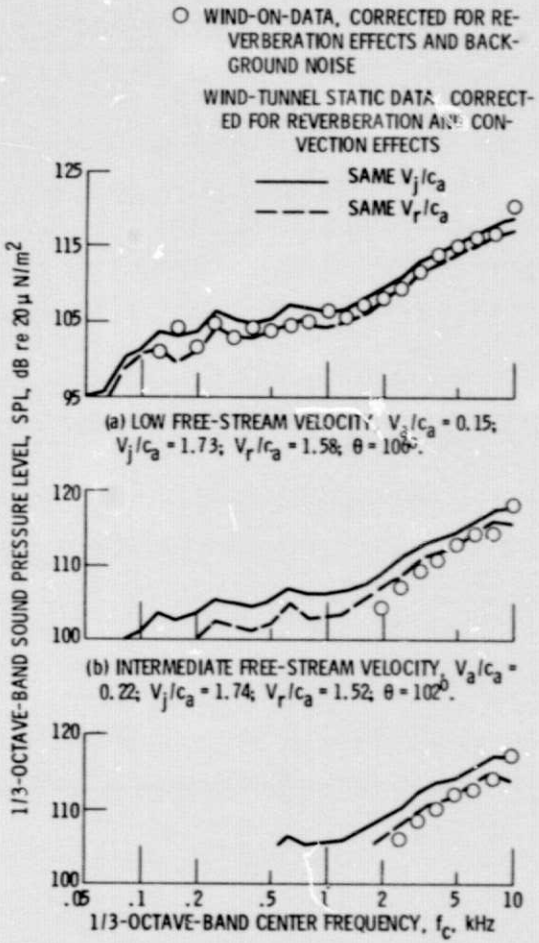

(a) LOW FREE-STREAM VELOCITY, $V_a/c_a = 0.15$; $V_j/c_a = 1.73$; $V_r/c_a = 1.58$; $\theta = 106^0$.

(b) INTERMEDIATE FREE-STREAM VELOCITY, $V_a/c_a = 0.22$; $V_j/c_a = 1.74$; $V_r/c_a = 1.52$; $\theta = 102^0$.

(c) HIGH FREE-STREAM VELOCITY, $V_a/c_a = 0.27$; $V_j/c_a = 1.71$; $V_r/c_a = 1.44$; $\theta = 100^0$.

Figure 9. - Effect of free-stream velocity on SPL spectra for 104-tube nozzle without shroud; high jet velocity; measurement angle, $\theta_m = 114^0$.

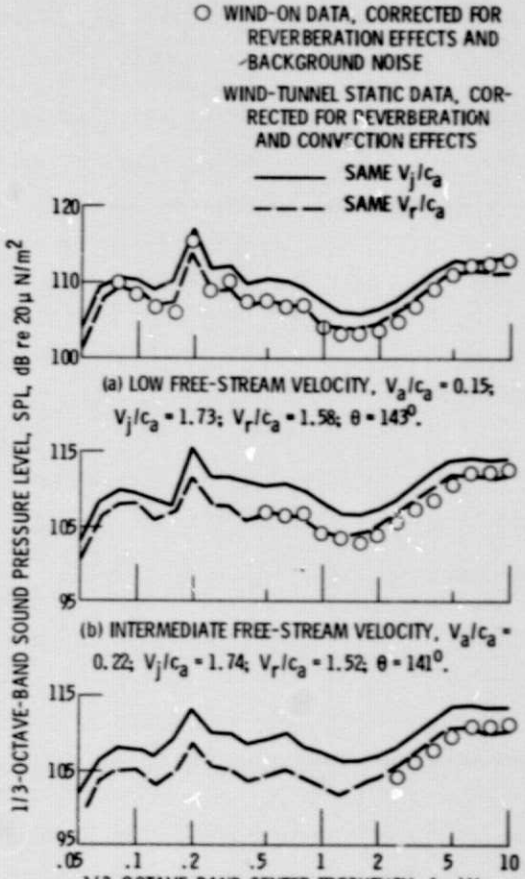

(a) LOW FREE-STREAM VELOCITY, $V_a/c_a = 0.15$; $V_j/c_a = 1.73$; $V_r/c_a = 1.58$; $\theta = 143^0$.

(b) INTERMEDIATE FREE-STREAM VELOCITY, $V_a/c_a = 0.22$; $V_j/c_a = 1.74$; $V_r/c_a = 1.52$; $\theta = 141^0$.

(c) HIGH FREE-STREAM VELOCITY, $V_a/c_a = 0.27$; $V_j/c_a = 1.71$; $V_r/c_a = 1.44$; $\theta = 140^0$.

Figure 10. - Effect of free-stream velocity on SPL spectra for 104-tube nozzle without shroud; high jet velocity; measurement angle, $\theta_m = 148^0$.

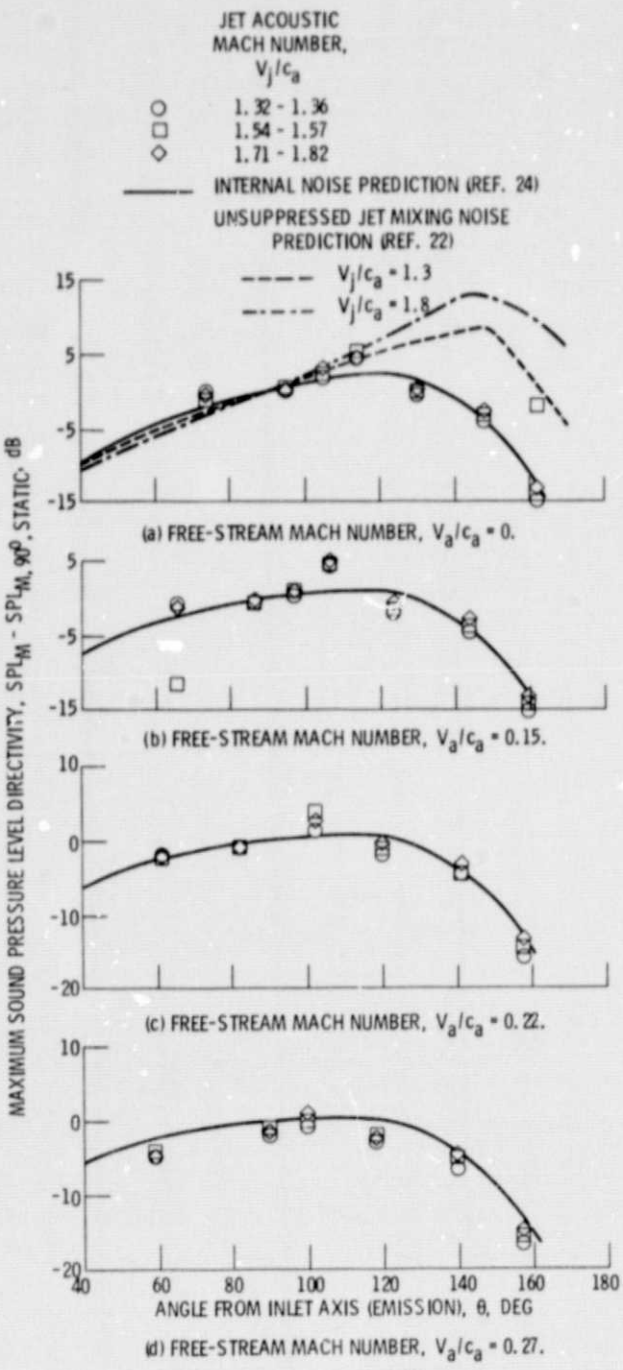

Figure 11. - Wind-tunnel sideline directivity patterns (maximum SPL) for 104-tube nozzle without shroud.

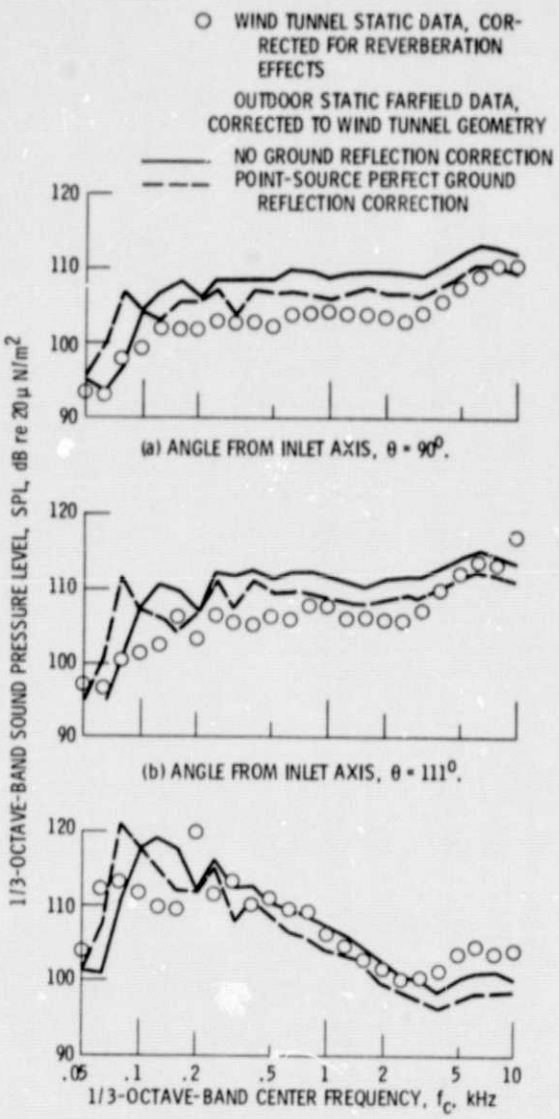

Figure 12. - Wind-tunnel nearfield effects for 104-tube nozzle with acoustically-treated shroud. Comparison of zero free-stream velocity data with outdoor farfield results; high jet velocity, V_j/c_a = 1.80.

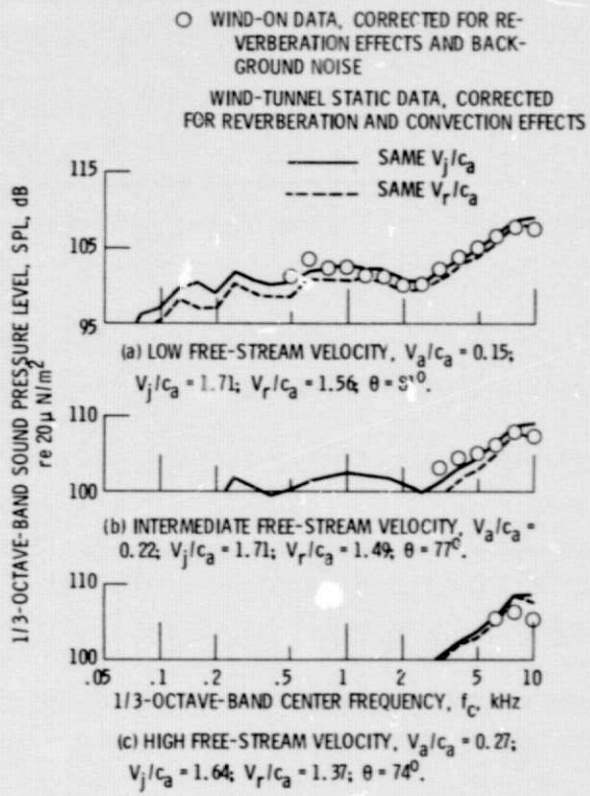

Figure 13. - Effect of free-stream velocity on SPL spectra for 104-tube nozzle with acoustically-treated shroud; high jet velocity; measurement angle from inlet axis, $\theta_m = 90^0$.

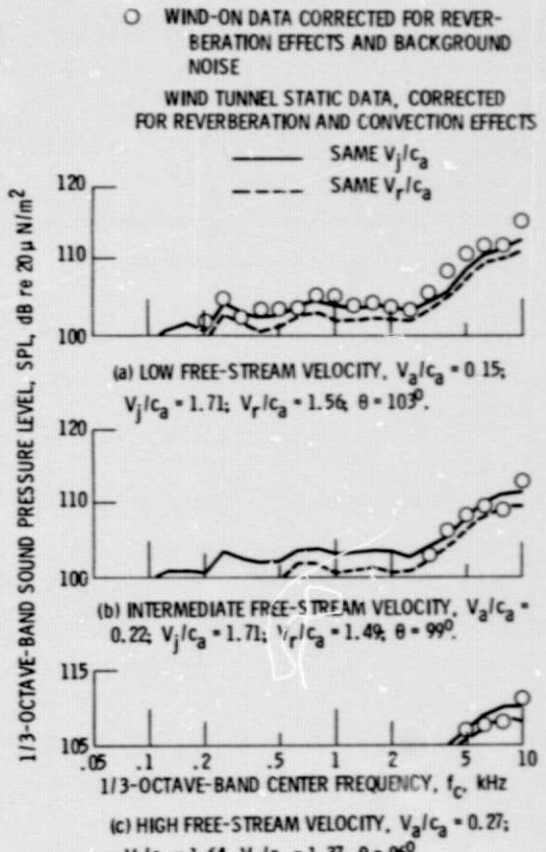

Figure 14. - Effect of free-stream on SPL spectra for 104-tube nozzle with acoustically-treated shroud; high jet velocity; measurement angle, $\theta_m = 111^0$.

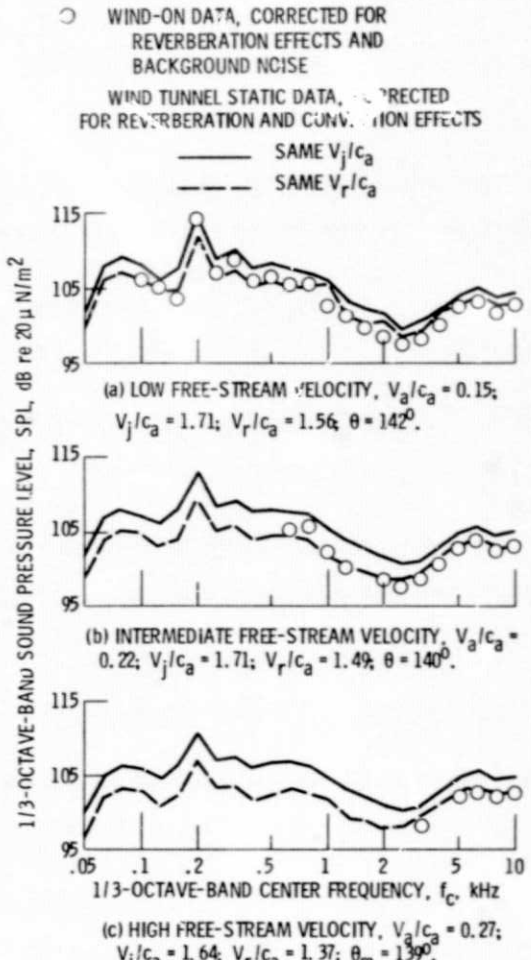

Figure 15. - Effect of free-stream velocity on SPL spectra for 104-tube nozzle with acoustically-treated shroud; high jet velocity; measurement angle, θ_m = 147°.

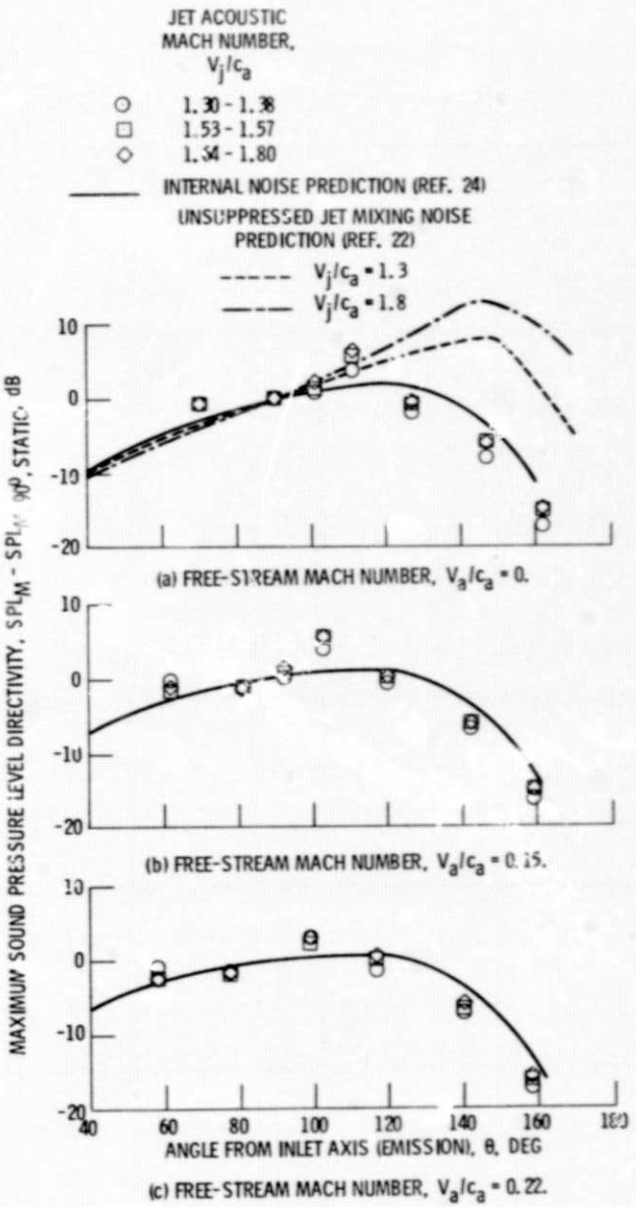

Figure 16. - Wind-tunnel sideline directivity patterns (maximum SPL) for 104-tube nozzle with acoustically-treated shroud.

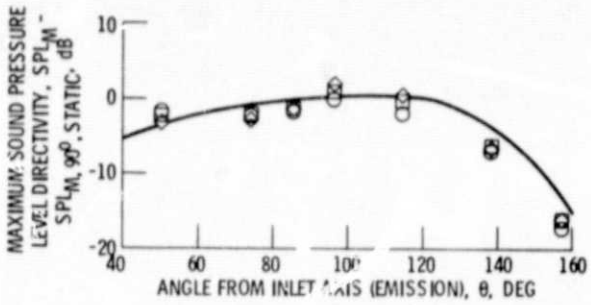

(d) FREE-STREAM MACH NUMBER, $V_a/c_a = 0.27$.

Figure 16. - Concluded.

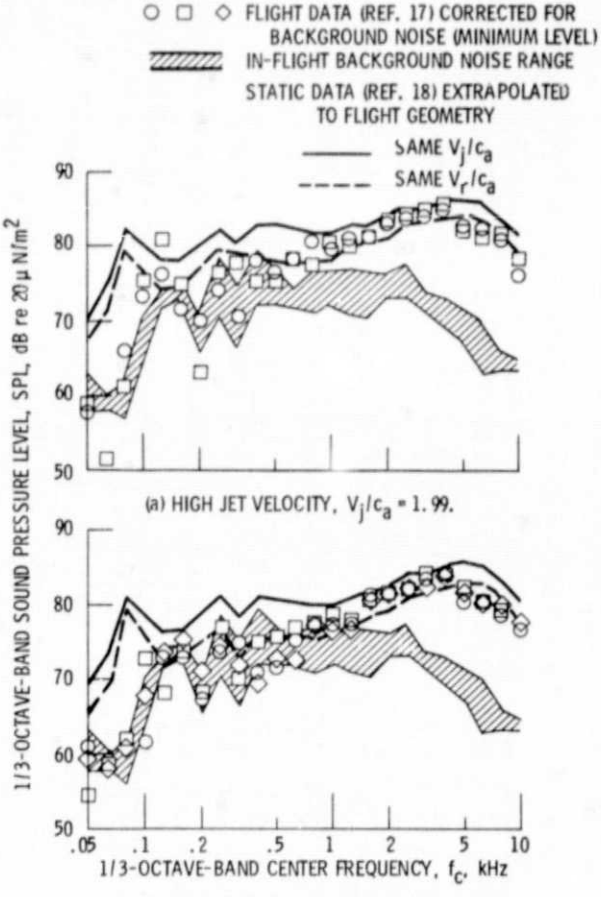

(a) HIGH JET VELOCITY, $V_j/c_a = 1.99$.

(b) INTERMEDIATE JET VELOCITY, $V_j/c_a \cong 1.82$.

Figure 17. - Effect of flight at $V_0/c_a \cong 0.37$ on SPL spectra for 104-tube nozzle without shroud, at emission angle $\theta \cong 90^0$; 91-m altitude level flyover, corrected to free-field.

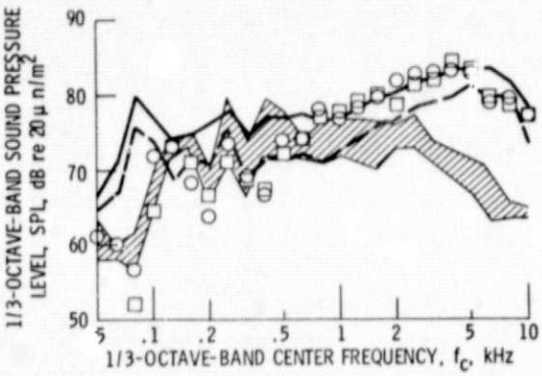

(c) LOW JET VELOCITY, $V_j/c_a \cong 1.54$.

Figure 17. - Concluded.

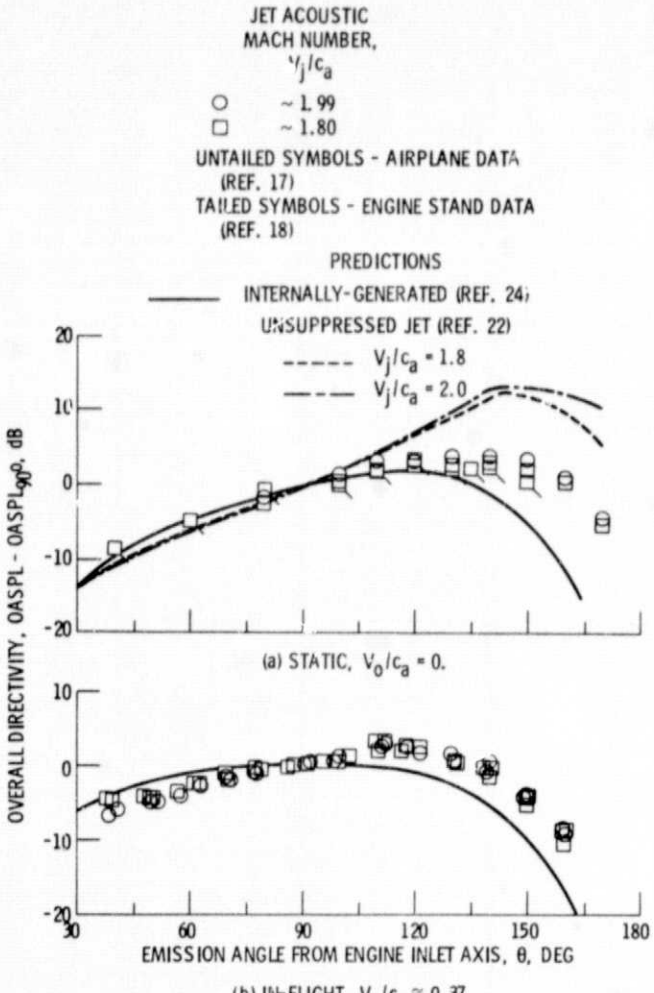

(a) STATIC, $V_0/c_a = 0$.

(b) IN-FLIGHT, $V_a/c_a \cong 0.37$.

Figure 18. - Level-flyover directivity patterns for 104-tube nozzle without shroud.

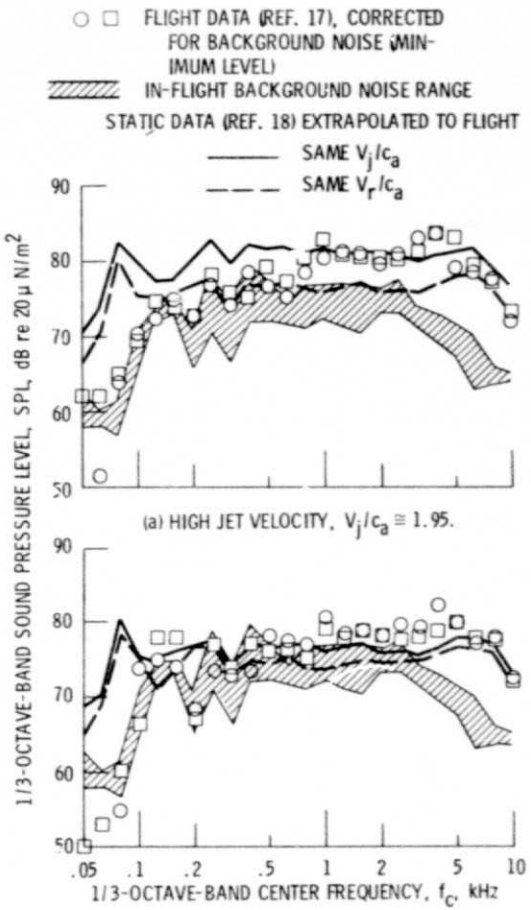

Figure 19. - Effect of flight at $V_0/c_a = 0.37$ on SPL spectra for 104-tube nozzle with acoustically treated shroud at emission angle $\theta \cong 90^0$; 91-m altitude level flyover, corrected to freefield.

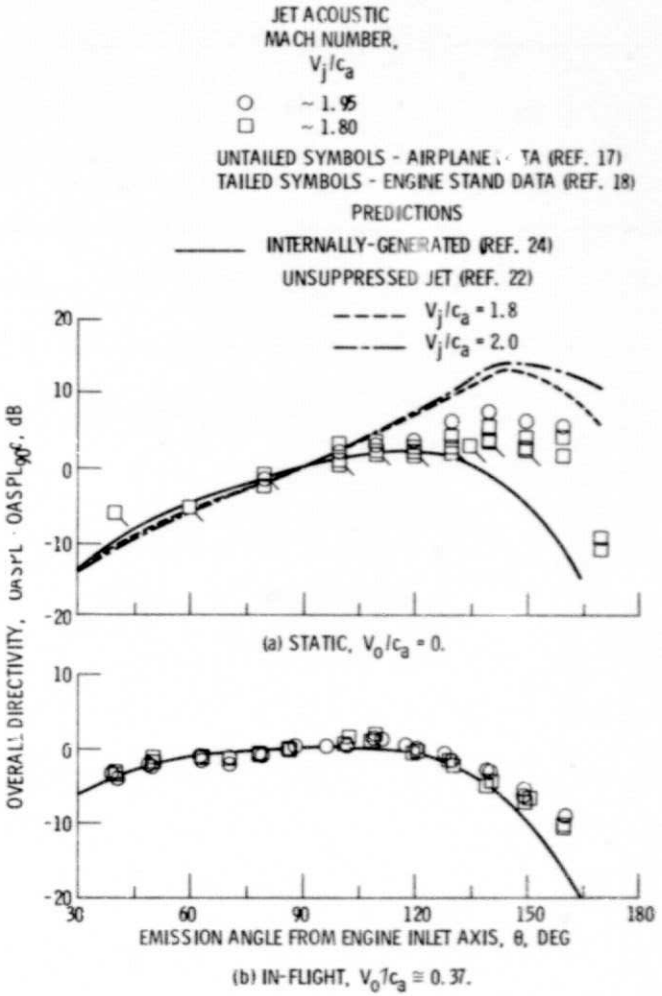

Figure 20. - Level-flyover directivity patterns for 104-tube nozzle with acoustically-treated shroud.